Proceedings of the ASME 2010 3rd Joint US-European Fluids Engineering Summer Meeting and 8th International Conference on Nanochannels, Microchannels, and Minichannels
FEDSM-ICNMM2010
August 1-5, 2010, Montreal, Canada

FEDSM-ICNMM2010-30094

Investigation of Scramjet Inlet Flow Using a Flux-Splitting Solver

D. M. Holian[(1)] and R. R. Mankbadi[(2)]
Embry-Riddle Aeronautical University, Daytona Beach, Florida
And the Florida Center for Advanced Aero-Propulsion Technology

ABSTRACT

A detailed analysis is carried out on a rectangular scramjet inlet to analyze the flow field. The focus is on examining boundary layer separation and shock interactions to ensure proper operation of the inlet. We developed herein a flux-splitting Navier Stokes solver to be used for optimizing the inlet geometry and operation conditions. The results seem to be in good agreement with that of FLUENT CFD software and explain the experimental results of Haberle (2008).

NOMENCLATURE

A_0 = Inlet capture area
C_d = Drag coefficient
C_p = Specific heat at constant volume
c_p = Pressure coefficient
M_∞ = Free stream Mach number
p_t = Total pressure
p_∞ = Free stream pressure
Re_m = Unit Reynolds number
T_t = Total temperature
T_∞ = Free stream Temperature
u, v, w = Velocity in the x-, y-, z- directions
ρ_∞ = Free stream Density

[1] Graduate Student
[2] Distinguished Professor, ASME Fellow

1. INTRODUCTION

Recent interest has been focused on developing hypersonic aircrafts for military purposes, civil transport, or as an alternative to the space shuttle system. Proposals to develop new propulsion systems to enable this technology have already been underway (Holland 1995 a, b & Sanders 2008). One such design is to use a turbofan for the initial takeoff and acceleration of the aircraft. Once supersonic, the engine would switch into its ramjet mode. This switch is performed by adjusting the cowls in the inlet configuration which directs the airflow into its proper path. After the aircraft has accelerated to Mach four, the turbofan-ramjet hybrid system shuts down completely enabling the scramjet system to take over. At this point, the cowl configuration has reached its final position which defines the final inlet geometry. In the positioning of these cowls, design constraints consist of allowing proper airflow to reach the combustion zone at specified velocities regardless of the free stream velocity and to limit the boundary layer separation. Furthermore, the inlet must be designed taking into consideration the shock waves interactions which would control the flow leading into the isolator and combustor.

Thus, to ensure the success of the turbine-based hypersonic engine, special attention is needed to ensure proper inflow to the engine (Huebner, 2000, Ramasubramanian, 2008, and Smart 2001). The configuration used for the computation is shown in figure 1. This corresponds to the test conditions at a flight Mach number of seven, which correlates with the experiment performed by Haberel (2008). The shock generation of the first ramp in the double ramped system causes boundary layer separation due to the large pressure gradient produced in the direction of the flow. After the second ramp, the flow is directed into the encased portion of the inlet in which its entrance is defined by a lip/cowl opposite of the ramp.

Our objective herein is to conduct a CFD analysis of the inlet flow to provide understanding of the thermal loading, the pressure distribution, the shockwaves interaction and the boundary layer separation to avoid an Unstart of the inlet (Berry 2004). This paper will illustrate where the location of problematic boundary layer separation forms and would then be a candidate position to place a passive boundary layer bleed.

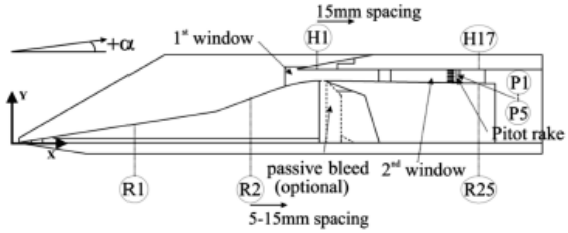

Figure 1
Side View of Inlet Model with Optional Passive Bleed (Haberle 2008)

2. NUMERICAL ISSUES

The geometry used in the computational analysis is based on the experimental model used in Haberle (2008) shown in figure 1. This model was first developed based upon the SCR-02 model which was altered by changing the internal contraction ratio to 0.16 forming the new GK-01 model. In terms of inlet parameters, the capture area A_0 of the model is 0.1 x 0.1 m^2, and the length L of the model from the beginning of ramp one to the combustion chamber is 0.585 m.

The governing equations are the compressible Navier-Stokes equations coupled with the energy equation. We have conducted two sets of computation: one using the commercial flow solver FLUENT; and we also developed our own flux-splitting flow solver. For the FLUENT solver, the flow is set based upon the experimental setup to be fully hypersonic at Mach seven. The explicit density based solver was used since it can accurately take into account the changes in density of the fluid within the flow field, and a local time-step was used. A first-order scheme is initially used, and then we switched to the third-order MUSCL. The flow was defined to be atmospheric air consisting primarily of oxygen and nitrogen with a ratio of one part oxygen to every 3.76 parts nitrogen. The flow parameters are: free stream Mach number = 7; pressure 170 Pa, temperature 46 K, density 0.0123 $kg \cdot m^{-3}$, total temperature 500; total pressure 7E5 Pa; unit Reynolds number 4.0 E6 m^{-1}.

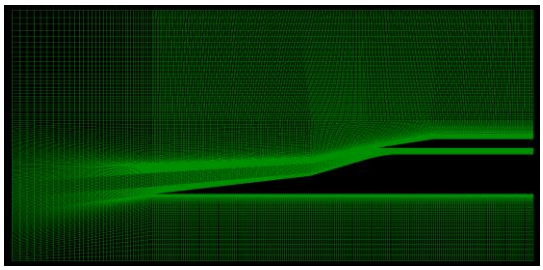

Figure 2
Structured Grid for Scramjet Inlet with Hypersonic Cowl Position

The computational grid was generated using Gridgen 15.10 (figure 2.). Due to the rectangular characteristics inherent in this inlet model, a structured grid was generated consisting of only quadrilaterals. The grid was efficiently designed using a minimal

number of cells. This was achieved by making the grid dense in specific areas, such as the boundary layer and inside the inlet's throat, and making the grid less dense elsewhere. Due to the flow being supersonic, upstream flow properties do not affect the downstream conditions; therefore, not much grid was needed in front of the inlet.

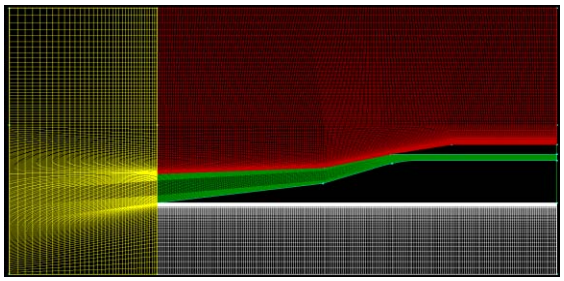

Figure 3
Final Zoning for Scramjet Grid

By creating multiple zones at specific locations, skewness can be minimized. For each face of the inlet, a zone was created with certain spacing along the wall which was kept at a constant width of five millimeters per each cell. These zones were then merged based on how they were connected together to form the entire grid consisting of now four zones as seen in Figure 3. The grid generated consists of 45,739 total cells. In regards to the cells in contact with the surface of the inlet, their thickness is 0.3 millimeters thick making them well within the boundary layer. Having ten to thirty cells is advisable in boundary layer regions to resolve the boundary layer.

2.1. Flux-Splitting Code: In addition to using FLUENT, we have also developed our own 2D flow solver in Fortran 90. Central difference was first attempted, but the shock waves were not captured within a reasonable number of iterations. So, we switched to a control-volume-based flux splitting approach by van Leer. The finite volume scheme implemented the Van Leer discretization method where the fluxes were split into an upwind and downwind portion denoted as plus and minus. These were then added together to form the corresponding flux at each face. It should be noted that the west wall of a given cell has identical magnitude but opposite sign flux as the east wall of the cell to its right. This is also true for the north and south walls.

$$F_E^{+} + F_E^{-} = F_E$$

For supersonic conditions, these fluxes are no longer split and each individual wall flux is calculated straight forward. This inherently lowers the order of the solver allowing for a fairly accurate method of capturing shocks. If the flow enters a subsonic region, then it switches back to the split flux technique.

2.2. Boundary Treatment: The top and bottom of the grid is defined as pressure farfield, the front portion of the grid is designated as an inflow, the rearmost sections are defined to be outflow, however the internal outflow condition seen in the combustor will be treated differently, and any solid part of the inlet will be defined as a viscous wall. This implies that the "u" and "v" velocities are set to zero at these points based on the no-slip condition. Furthermore, since pressure is defined to be constant within the boundary layer, both the pressure and the density will be linearly extrapolated based on the surrounding nodes. The method of characteristic was used to implement the inflow & outflow boundary conditions. Three parameters are defined and one is extrapolated from the interior computational domain. However, in supersonic cases, these equations simplify to pressure farfield conditions. This is due to the fact that the pressure wave travels slower than the overall flow field thereby not allowing the inflow boundary nodes to receive any propagated information from its neighboring nodes. These physical conditions are important to consider for an

accurate representation of the flow properties. The basic outflow discretization is similar to inflow, being based on the method of characteristics. However, all information is set to the upstream condition based on supersonic assumptions. Using this boundary treatment for the outflow inherently takes care of the behavior inside the inlet.

Zonal Interactions: Due to the use of a multi-zone grid, two problems arise that must be addressed. The first being artificial boundaries generated by the grid. It is obvious that in Figure 3, the yellow zone has an outflow which is equivalent to the white zone's inflow. This could be achieved by treating one as an outflow condition and then setting this as the inflow of another zone. However, this would be a tedious and inefficient process. Instead, information just before the interface from zone one and just after the interface from zone two will be used in accordance to central differencing to determine the information at the interface. The second problem is nodal overlapping. Physically, the last node of zone one is the same point as the first node of zone two. However, mathematically, these are stored as two separate points. To account for this, all that is done is the information found for the outflow node of zone one is set equal to the corresponding nodal information at the inflow of zones two.

Shock Capturing (ENO): The scheme at hand has a tendency to blur discontinuities over several nodes. To accurately account for the shock, the Essentially Non-Oscillatory scheme (ENO) is used. An ENO scheme allows the computational stencil to adapt to given flow properties. By analyzing these properties, the scheme can lower the order of the stencil to just a basic first order up winding scheme allowing it to sharply capture the discontinuity. Once away from the discontinuity, the order of the scheme is increased to its original order until another switch is detected. This is why this scheme is also known as a pressure switch.

3. RESULTS

Fluent: We present herein two runs for Fluent. One using a first-order upwind scheme, the second, using the MUSCL scheme. Both cases are laminar as the turbulence model seemed to have little effect on the flow encompassing the bleed location and shockwave interaction. Due to this, a direct comparison between Fluent and the developed flux splitting solver could be formed. The convergence limit was set to E-03 however the L2Norms never reached that limit because of the inherent complexity. Determining the point of convergence was achieved by viewing the corresponding coefficient of drag on the scramjet inlet. When the value no longer varied, it could be assumed that convergence has been reached. Figure 4 clearly illustrates convergence after roughly 450 iterations with a C_d value of 0.025.

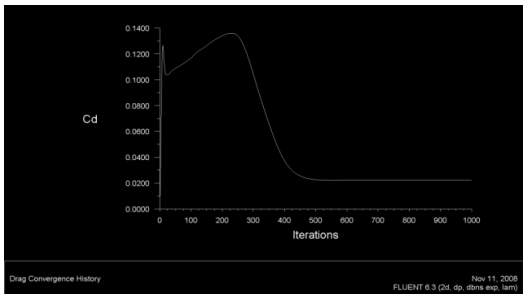

Figure 4
C_d Convergence History First-Order Laminar

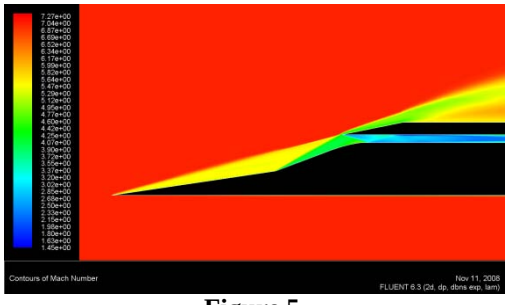

Figure 5
Mach Contours for First Order Laminar

Figure 5 illustrates the shock formation occurring throughout the inlet. It should be noted that the shock line created off the second ramp just meets the tip of the cowl but does not hit inside of it. This was a design parameter performed in the experimental setup in order to decrease the shock-shock interactions. Figure 6 demonstrates the change in pressure across the shock lines and the spike in pressure at the tip of the cowl and towards the combustion chamber in the rear of the inlet. While these first order results are not exact, they yield a general idea of what the flow field looks like.

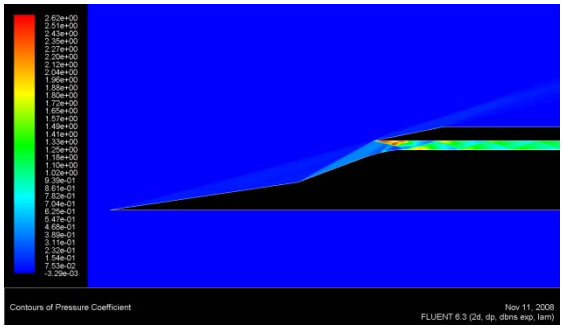

Figure 6
Coefficient of Pressure Contours for First Order Laminar Computation

Next, we modified the fluent runs to the third-order MUSCL scheme to provide a more accurate representation of the previous case because it takes into consideration the discretized terms up to the third order. Although initial values were given based of the first-order run, convergence still needed to be fully determined before one could assume the results were correct.

The results are modified slightly as shown in figure 7. One thing to note in the figure is that just before the flow field reaches the inlet's throat along the bottom wall an expansion wave forms. This is a tiny and localized point in the flow field where the velocity is actually increasing to a Mach number of ten. This is also the point just before the separation of the boundary layer

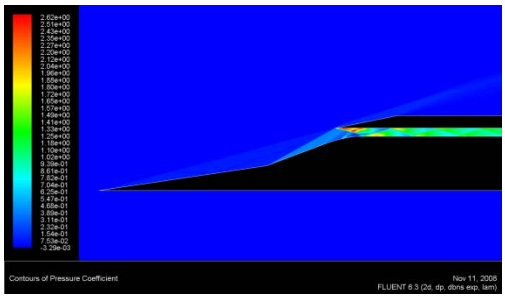

Figure 7
Coefficient of Pressure Contours for Third Order Laminar Computation

begins and the point where the passive bleed has been proposed to be inserted in order to reduce the boundary layer separation. Figure 7 also shows that the coefficient of pressures in this 3rd-order run varies more in comparison to the first order approximation as can be seen in the first Mach zone connected to the lip of the inlet.

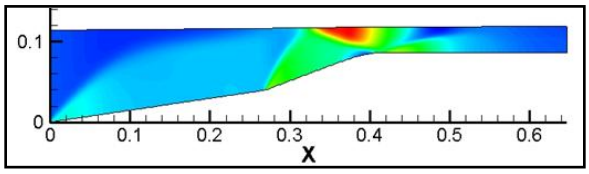

Figure 8
Pressure Contour Van Leer

Finite Volume Van Leer Solver: The Van Leer finite volume scheme, due to its inherent ability to capture shocks by lowering adjusting the local stencil, provided fairly accurate results at the beginning of the inlet (figure 8). However, the solver did not accurately solve the outflow condition. It was also unable to capture all of the reflecting oblique shocks. This is primarily due to shock wave interaction which the code was not able to handle. Figure 8 illustrates that at the point where the shocks are first going to interact, the code eliminates them. Although the internal shocks were not all captured, it is clear that the solver can handle portions of

the hypersonic flow as is. Further considerations should include chemically reacting flows as is the case in hypersonic conditions. Also, the specific heats are not going to be constant as assumed here. Sutherland's law also has limitations and while used, isn't accurate at hypersonic speeds. Finally, a turbulence model should be included to help stabilize the boundary layer which may be another primary factor in the shock dissipation.

4. COMPARSION WITH EXPERIMENT

The first comparison that will be made is a visual comparison of shock formation. This is done by comparing the shock lines seen in the Mach contours of the CFD results and the experimental Schlieren photography (figures 9 & 10).

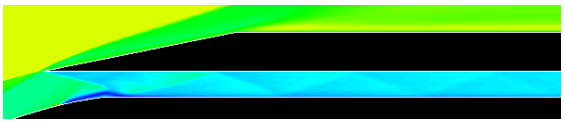

Figure 9
Mach Contours for Third Order Laminar Computation Fluent

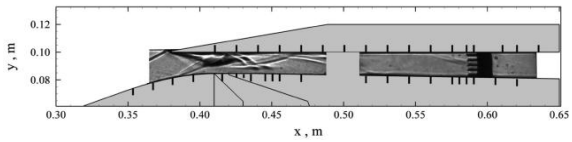

Figure 10
Schlieren Photograph of Flow field (Haberle 2008)

The Mach line formations are almost at the exact same position. Furthermore, alternating shock formations (based on the differing shades of blue) can be seen in the first shock zone connected to the inlet lip. The Schlieren photograph also portrays this by showing the alternating shock lines within that zone. One other difference that should be noted is that Fluent predicted the initial separation of the boundary layer slightly prior to the experimental results.

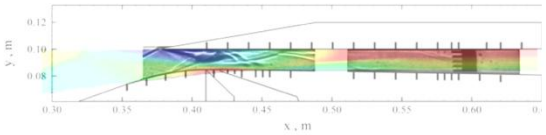

Figure 11
Solver Contour versus Experimental (Haberle 2008)

Figure 11 illustrates the experimental Schlieren photograph translucently set on top of the mach contours produced by the finite volume solver. It can be seen that in the front of the inlet, the solver predicted the location and the angles of the mach lines extremely accurately. The main point of interest is the separation occurring on the bottom ramp going into the inlet. This matched almost exactly with the experimental results. Therefore, it can be stated that a laminar assumption is a valid procedure for this design.

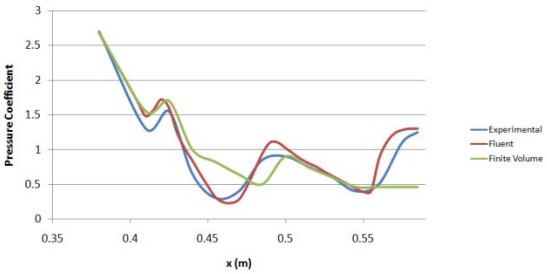

Figure 12
Pressure Coefficient Comparison

Figure 12 demonstrates the comparison of the coefficients of pressure along the top wall of the inlet for the CFD models and experimental results. It can be seen that the results generated by Fluent in comparison to the experimental results are extremely similar. When comparing this plot to the Mach contour plot, it can be seen that the jumps in pressure occur just after the formation of a shock line. Then, the pressure dissipates until the next shock occurs resulting in another spike in pressure.

The finite volume solver follows the trend extremely well to begin with until the first shock interaction. The results, as seen in the previous pressure contours which are blurred just after the inlet opening, show a variance in comparison to the experimental values and Fluent's. The trend then gets more accurate until it can no longer pick up the rearward Mach interactions thereby leveling off the pressure coefficients at a low value.

5. CONCLUSIONS

Through the use of the fluent solver and the developed flux-splitting finite volume code, a fairly accurate description of the Mach seven hypersonic inlet was generated. This was done by incorporating a density-based, explicit scheme solver under ideal gas conditions and implementing them with a third order, laminar model. Increasing the order from first to third demonstrated a more accurate representation of the viscous terms. When comparing the Mach contours and the pressure coefficients generated by Fluent and the solver to those created in the experiment illustrated that the CFD solvers, especially Fluent, yielded accurate results. This would warrant the use of this setup with varying conditions such as free stream pressure, temperature, and/or Mach number.

Also, the formation of the boundary layer separation bubble warrants extra inlet modifications such as a passive bleed port (Berry 2004). Using such a port can greatly reduce the separation which increases the overall efficiency of the inlet. Although the experimental model was performed and stated as a two-dimensional system, it is actually three-dimensional. More accurate CFD models could be generated by creating a true three-dimensional system, as well as incorporate the shock interactions generated by the side walls as well as the top and bottom walls. This combined with the physical behavior of hypersonic flows, including chemically reacting conditions, will tremendously increase the accuracy of the system.

Acknowledgments

This work was supported by the Florida Center for Advanced Aero-Propulsion. Special thanks to William K. Barcza and Dean Andreas of Pratt and Whitney Rocketdyne for providing valuable input.

REFERENCE

1. Berry, S. A., Boundary Layer Control for Hypersonic Air breathing Vehicles," AIAA-*2004-2246.*
2. Haberle, J. "Investigation of Two-Dimensional Scramjet Inlet Flow field at Mach 7," AIAA-*33545-641,* Journal of Propulsion and Power Vol. 24, No. 3, May-June 2008.
3. Holland, S. D. "Mach 10 Computational Study of a Three-Dimensional Scramjet Inlet Flow Field," NASA *TM 4602*, 1995 Langley Research Center, Hampton, Virginia.
4. Holland, S. D. "Mach 10 Experimental Database of a Three-Dimensional Scramjet Inlet Flow Field," NASA *TM 4648*, 1995 Langley Research Center, Hampton, Virginia.
5. Huebner, L. D., Kenneth, R., Witte, D., Ruf, E., and Andrews, E., "Hyper-X Engine Testing in the NASA Langley 8-Foot High Temperature Tunnel," AIAA 2000-3605.
6. Ramasubramanian, V., "Numerical Simulations of Busemann Hypersonic Inlets at Finite Flight Angles," AIAA *2008-7497.*
7. Sanders, B. W. "Aerodynamic Design of a Dual-Flow Mach 7 Hypersonic Inlet System for a Turbine-Based Combined-Cycle Hypersonic Propulsion System," *AIAA 2008-030015, NASA/CR—2008-215214.*
8. Smart, M. K. "Experimental Testing of a Hypersonic Inlet with Rectangular-to-Elliptical Shape Transition," AIAA-*5774-978*, Journal of Propulsion and Power, Vol. 17, No. 2, March-April 2001.